Graphene on SiC(0001) and SiC($000\bar{1}$) Surfaces Grown via Ni-silicidation Reactions

T. Yoneda[1], M. Shibuya[2], K. Mitsuhara[2], A. Visikovskiy[2], Y. Hoshino[3] and Y. Kido[2,*]

Abstract

This paper presents the structure and electronic properties of graphene grown on 6H-SiC(0001) and SiC($000\bar{1}$) surfaces via Ni-silicidation reactions at temperatures around 800°C. Silicidation reactions take place at temperature higher than 400°C for Ni(10 ML)/SiC and a single-phase θ-Ni_2Si(0001)-layer grows epitaxially on SiC($000\bar{1}$) at 500°C, whereas a mixed phase silicide-layer is formed on the SiC(0001) substrate. Annealing at 800°C leads to growth of ordered graphite layers on both SiC($000\bar{1}$) and SiC(0001) surfaces with an areal occupation ratio of ~65 %, which surround the Ni-silicide islands. High-resolution ion scattering analysis reveals that single- and double-layer of graphite grow on the SiC($000\bar{1}$) and SiC(0001), respectively. The dispersion curve of the π band for the double-layer graphite(DG) on the Si-face lies about 1 eV above that of the single-layer graphite(SG) on the C-face around the Γ-point. The work functions of the SG/SiC($000\bar{1}$) and DG/SiC(0001) are derived to be 5.15±0.05 and 4.25±0.05 eV, respectively, which coincide well with the theoretical prediction based on the *ab initio* calculations. The present results indicate that the electronic states of graphene are influenced by the interaction with supports.

[1] *Department of Electric Engineering, Fukui National College of Technology, Sabae, Fukui-ken 916-8507, Japan*

[2] *Department of Physics, Ritsumeikan University, Kusatsu, Shiga-ken 525-8577, Japan*

[3] *Department of Information Science, Kanagawa University, Hiratsuka, Kanagawa 259-1293, Japan*

1. Introduction

The single-layer of ordered graphite usually called "graphene" has now attracted much attention for its conspicuous electronic properties[1-2]. Indeed, a single-layer graphene (SG) provides a perfect two-dimensional electron gas with a much higher electron density and mobility than those of compound semiconductor hetero-junctions[3-7]. In addition, it has been predicted that a graphite ribbon gives a characteristic electronic state near the Fermi level (E_F) so called the edge localized state dependent strongly on the edge shape such as zigzag and armchair type[8-10]. The π (bonding) and π*(anti-bonding) states of graphene forming the highest occupied VB (valence band) and lowest unoccupied CB (conduction band), respectively are very sensitive to the lattice symmetry and give a number of unusual electronic transport properties[1,3-5].

Up to now, some methods have been proposed so far to form graphene, such as (i) mechanical exfoilation from bulk graphite crystal[1-4], (ii) thermal decomposition of ethylene gas on Ni(111) and TaC(111) substrates at high temperatures in ultrahigh vacuum (UHV)[11,12] and (iii) heating SiC(0001) and SiC($000\bar{1}$) surfaces at ~1500˚C in UHV[5-7, 13,14]. Now, it is widely recognized that the method to grow single (SG) and double (DG) layer graphene layers on SiC(0001) and SiC($000\bar{1}$) is the most popular and controllable technique. We reported previously growth of ordered graphite layers with double domains by annealing Ni-deposited 6H-SiC(0001)[15]. The aim of this paper is to characterize more precisely the atomic and electronic structures of Ni/SiC(0001) and Ni/SiC($000\bar{1}$) which are annealed in UHV. Our primary concern resides in how to control the thickness of ordered graphite layers and the electronic states of SG and DG dependent upon underlying SiC faces. The analysis is carried out by high-resolution medium energy ion scattering (MEIS) combined with photoelectron spectroscopy (PES) using synchrotron-radiation-light. Growth of ordered SG and DG is identified by reflective high energy electron diffraction (RHEED), high-resolution MEIS, valence band and C 1s core level spectra. The band dispersions and work functions for the SG and DG on SiC(0001) and SiC($000\bar{1}$) substrates are also measured and compared with the theoretical prediction based on the first principles calculations[16,17].

2. Experimental

The samples used here are N-doped (1×10^{18} N/cm^3) 6H-SiC(0001) and 6H-SiC($000\bar{1}$) substrates treated by chemical and mechanical polishing which were purchased from CREE Inc. After cleaning the surface by a modified RCA method[18], the sample was immediately introduced into an UHV chamber and degassed at 600°C for 5 h. In order to suppress a partial surface graphitization we deposited a small amount of Si (3 – 5 ML, 1 ML: 1.21×10^{15} atoms/cm^2) on the surface at room temperature (RT) and then annealed the sample at 950°C and 1000°C for 5 min in UHV to form 6H-SiC($000\bar{1}$)-2×2 and 6H-SiC(0001) - $\sqrt{3}\times\sqrt{3}$ surfaces, respectively, which were

confirmed by RHEED[19]. After cooling down to RT, Ni was deposited on the clean surfaces by molecular beam epitaxy (MBE) at a rate of ~1 ML/min. We used infrared radiation to heat up samples, which was focused by a concave mirror and then introduced into a sample preparation chamber after transmitted through a quartz rod. A Pt/Rh thermocouple wire inserted between the quartz rod and a sample surface measured annealing temperature with an uncertainty of ±20°.

High resolution-MEIS using a toroidal electrostatic analyzer (ESA) determined the absolute amounts of Ni deposited and graphite(C) grown on a surface and the elemental compositions of Ni-silicides formed by annealing in UHV. In the present MEIS spectrum analysis, we employed the ZBL potential[20] to calculate scattering cross sections and the energy straggling values given by Lindhard-Scharff[21]. The stopping powers of C, Si and Ni as well as He^+ fraction dependent on emerging energy and surface materials were measured in advance using their thin films (C/LiF, Si/HOPG, Ni/SiO_2/Si, HOPG: highly oriented pyrolytic graphite). An exponentially modified Gaussian (EMG) distribution was used as the line shape of scattered He^+ ions[22]. We measured C 1s and Si 2p core levels as well as valence band spectra at photon energies of 390, 140 and 40 eV, respectively using a hemispherical ESA. Work functions were also determined from secondary electrons by 140 eV photon impact on samples which were negatively biased. The energy of the SR photons were calibrated with a grating covering photon energy 20 - 150 eV using primary and the 2nd harmonic waves for Au $4f_{7/2}$ line, whose binding energy (E_B) was assumed to be 84.0 eV. In the case of another grating for higher photon energy up to 500 eV, we set the E_B value of C 1s of SiC at 283.0 eV. The sample preparation and all the analyses mentioned above were carried out *in situ* under ultrahigh vacuum conditions ($\leq 3\times10^{-10}$ Torr).

3. Results and Discussion

The structure and phase of Ni-deposited SiC(0001) and SiC($000\bar{1}$) before and after annealing are dependent upon Ni thickness[15, 19, 23]. In the previous papers [15,19], we reported the growth modes of silicides and formation of graphite layers on 6H-SiC(0001) for Ni thickness of 5 and 10 ML at annealing temperatures ranging from 500 to 800°C for 2 min in UHV. This paper compares the initial silicidation reactions together with growth of graphene taking place on Ni(10 ML)/6H-SiC($000\bar{1}$) with those for Ni/6H-SiC(0001). Our concern is centered on differences of the structures and electronic properties of the graphene grown on Si- and C-terminated SiC(0001) surfaces, which will be presented below via precise analysis of MEIS and measurement of work functions etc.

3-1. Growth modes

Figure 1 shows the MEIS spectra observed for Ni(10 ML)-deposited SiC(0001) and SiC($000\bar{1}$) as-grown and annealed at 400(450) and 500°C. Here, 120 keV He^+ ions were incident at an angle of 54.7° and scattered to 54.7° with respect to surface normal, corresponding to a double alignment

geometry. Compared with corresponding random MEIS spectra from Ni (not shown here), growth of uniform and epitaxial Ni layers is unambiguous for both as-deposited samples in spite of a large lattice mismatch of 19 %. The MEIS spectra from Ni without tails indicate thickness uniformity of the Ni-layers. RHEED observation (not indicated here) also confirmed epitaxial growth of double-domain Ni(111) layers (*i.e.* Ni(111)-[$1\bar{1}0$]//SiC-[$11\bar{2}0$]: major, Ni(111)-[$11\bar{2}$]// SiC-[$11\bar{2}0$]: minor). The MEIS spectra from Si show small surface peaks (indicated by arrows in Fig. 1) and inclusion of Si in the Ni lattices, indicating diffusion of Si atoms initially forming the $\sqrt{3}\times\sqrt{3}$ reconstruction (Si adlayer: 1/3 ML) together with the Si atoms of the top Si-C bilayer for SiC(0001) and of those making the initial 2×2 surface reconstruction (1 ML) for SiC($000\bar{1}$)[23]. The aligned MEIS spectra from Si are deconvoluted into three components (diffused on top and into Ni-lattices and SiC substrate), as shown for Ni/SiC(0001) previously[19]. Such epitaxy of Ni layers is probably due to the fact that the diffused Si atoms act as a kind of surfactant. Concerning the as-deposited samples, there is no significant difference between Si- and C-terminated surfaces,

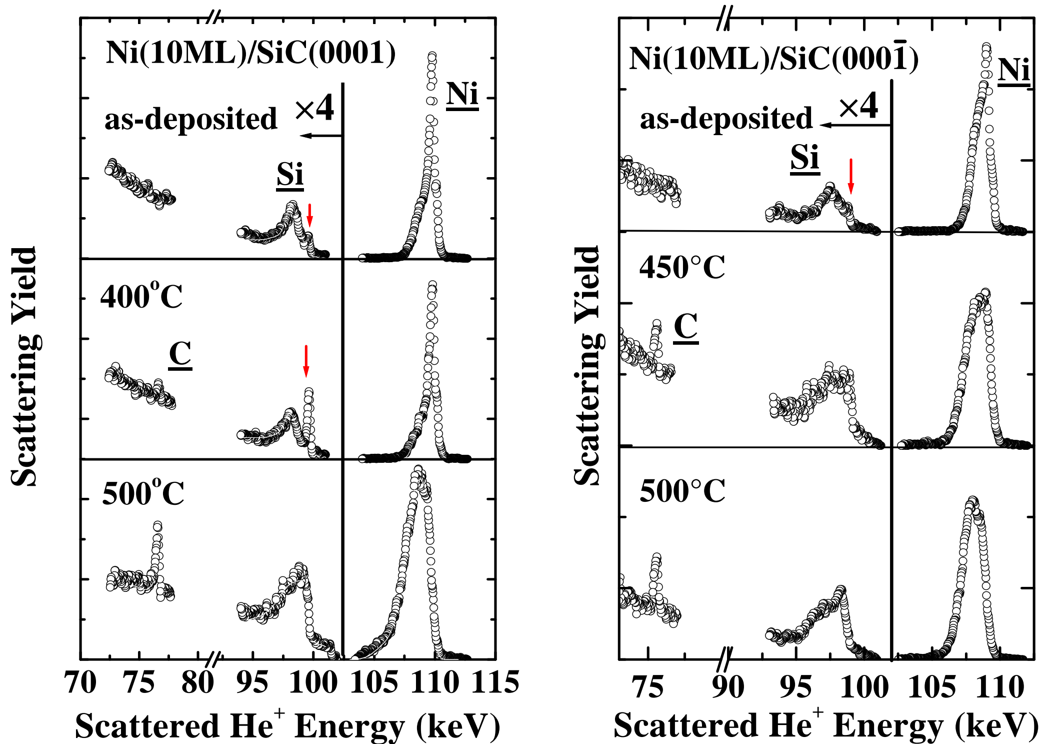

Fig. 1. MEIS spectra observed for 120 keV He^+ ions incident on Ni(10 ML)/SiC(0001) as grown and annealed at 400 and 500°C (left) and Ni(10 ML)/SiC($000\bar{1}$) as grown and annealed at 450 and 500°C (right). Incident and detection angles are −54.7 and 54.7°, respectively with respect to surface normal. (If we regard 6H-SiC(0001) as a cubic crystal (good approximation), the (0001) and the incident and detection angles of −54.7 and 54.7° correspond to [111]-, [100]- and [010]-axis, respectively).

except for the amounts of Si diffused into Ni-lattices and on top of the surfaces. A smaller amount of the diffused Si (~1 ML) for the SiC($000\bar{1}$) than that (~4/3 ML) for SiC(0001) which were derived from detailed analysis of MEIS spectra from Si probably degraded the crystallinity of the epitaxial Ni-layers on the C-face (larger areal intensity of the Ni spectrum for the C-face).

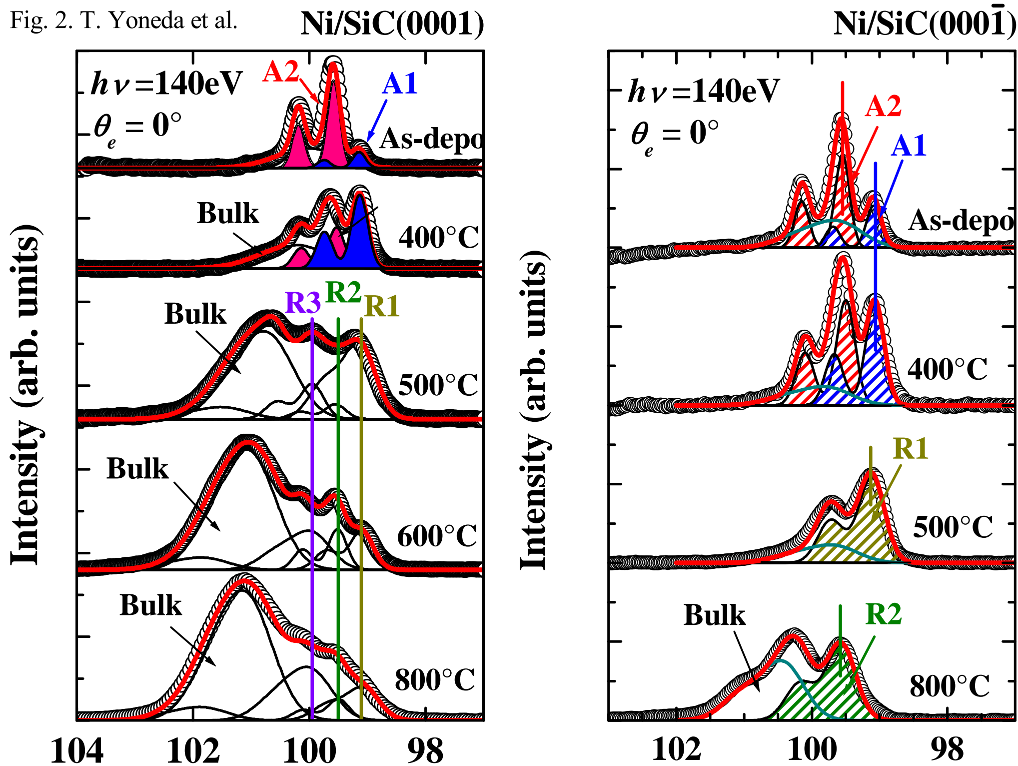

Fig. 2. Si $2p_{1/2,3/2}$ core level spectra observed at photon energy of 140 eV for Ni(10 ML)/SiC(0001), as grown and annealed at 400, 500, 600 and 800°C (left) and for Ni(10 ML)/SiC($000\bar{1}$), as-grown and annealed at 400, 500 and 800°C (right). A1 and A2 denote the components of Si atoms segregated on top of the surface and diffused into Ni lattice, respectively. R1, R2 and R3 originate from Ni_2Si, NiSi and $NiSi_2$, respectively, which were identified by the spectra observed for the standard samples of Ni_2Si, NiSi and $NiSi_2$ stacked on 6H-SiC(0001).

The two components of Si diffused into Ni-lattices and on top of the surfaces were clearly seen in Si 2p core level spectra (Fig. 2), which were previously assigned for Ni/6H-SiC(0001) as A1(surface-segregated) and A2(included in Ni lattices)[15,19]. After annealing at 400°C for 2 min there still exist Ni layers and the surface diffusion is strongly promoted for both samples. The strongly increased Si surface peak in the MEIS spectra is well correlated with the increase in the component A1 in the Si 2p spectra. At temperatures above ~450°C Ni-silicidation reaction takes place and C atoms are diffused on the surfaces for both SiC(0001) and SiC($000\bar{1}$). Annealing at 500°C leads to formation of a uniform and epitaxial layer of single phase Ni_2Si (identified by

RHEED and Si 2p core level shifts) which is covered with a thin C layer for SiC($000\bar{1}$)(see Figs. 1 and 2). The strong and sharp C peaks and the Ni spectra without tails in the MEIS spectra, respectively evidence location of the C-layers on top and formation of uniform Ni_2Si (average) layers. In the case of SiC(0001), the Ni_2Si phase is dominant but small amounts of NiSi and $NiSi_2$ are included, which are indicated by R1(Ni_2Si: primary), R2(NiSi) and R3($NiSi_2$), respectively in Fig. 2. The MEIS spectrum from Ni for annealing at 500°C has a tail, indicating thickness non-uniformity of the Ni-slicide layers, which causes an increase in the bulk component of Si 2p (see Fig. 2; left column). RHEED observation (not shown here) for the Ni/SiC(0001) and Ni/SiC($000\bar{1}$) annealed at 500°C showed the patterns corresponding to growth of epitaxial θ-Ni_2Si(0001) (hexagonal: a = 0.38 nm, c = 0.489 nm [24]) layers. The exact phase identification was performed by preparing standard samples of Ni_2Si, NiSi and $NiSi_2$ formed by co-deposition of Ni and Si on SiC(0001) substrates. The binding energy (E_B) of Si $2p_{3/2}$ for Ni_2Si, NiSi and $NiSi_2$ observed are 99.1, 99.4 and 99.9 eV, respectively with uncertainty of ±0.1 eV, which coincide well with the previous reports[25,26]. The lower binding energy shifts of the bulk component (as-deposited and 400°C annealing and 500°C annealing for SiC($000\bar{1}$)) were caused by Schottky contact (upward band bending). Aside from clear RHEED patterns from the ordered Ni-silicides layers, weak spots from graphite were observed for both substrates annealed at 500°C. From the MEIS spectra (Fig. 1), about a half of the surfaces were covered with single-layer graphite.

The interfacial reactions and surface morphology for Ni/6H-SiC($000\bar{1}$) are almost the same as those for Ni/6H-SiC(0001) at annealing temperatures up to 500°C, except for the fact that single-phase θ-Ni_2Si(0001) layers grow on SiC($000\bar{1}$), while mixed phase Ni-silicide (Ni_2Si + NiSi + $NiSi_2$) layers on SiC(0001). Such a difference probably comes from different rates for the reaction of Ni with Si-C and C-Si bi-layers.

3-2. Growth of Graphene

Annealing at higher temperatures leads to growth of ordered graphite layers (graphene) which surround Ni-silicide islands for both Si- and C-terminated substrates. Indeed, RHEED patterns (not shown here) clearly indicated ordered graphite layers with a double domain structure for both substrates, namely (i) a-axis of graphite is parallel to that of SiC(0001) and (ii) a-axis of graphite is rotated by 30° from that of SiC(0001). Note that twice the C-C bond length of graphite (1.42 Å) mismatches the lattice parameter a of SiC(0001) (3.08 Å) only 7 %. From the RHEED line intensity, the latter domain (ii) is dominant. In this case, good lattice matching is realized, if the graphene takes a $\sqrt{3}\times\sqrt{3}-R30^\circ$ unit cell, where the C-C bond length is dilated by 8 %. . Figures 3 (a) and (b) show the MEIS spectra observed for Ni(10 ML)/SiC(0001) and Ni(10 ML)/SiC($000\bar{1}$) annealed at 800°C for 2 min in UHV. The observed spectra are best-fitted assuming formation of Ni-silicide islands with an average elemental composition of Ni/Si = 1 and

the islands surfaces covered with thin Si-rich silicide layers (Ni/Si=1/2, average thickness: 5×10^{15} atoms/cm^2) on SiC(0001) and with extremely thin Ni layers (0.3×10^{15} atoms/cm^2: ~0.25 ML) atop the NiSi layers on SiC($000\bar{1}$). In both substrates, the areal occupation ratio of the Ni-silicide islands is ~35 %, which was estimated by an atomic force microscope. The islands are surrounded by thin C layers, because the C peaks in the MEIS spectra are very sharp, indicating the C-layers on top. The possibility of graphene sitting on the silicides islands is unlikely, because epitaxial graphene layers were evidenced by RHEED (graphite-[$1\bar{1}00$]//SiC-[$11\bar{2}0$]: dominant) as mentioned before and the silicides islands are randomly oriented in the lateral direction, as confirmed by MEIS and RHEED (patterns observed are from SiC(0001)-1×1 and graphite only). Figure 4(a)

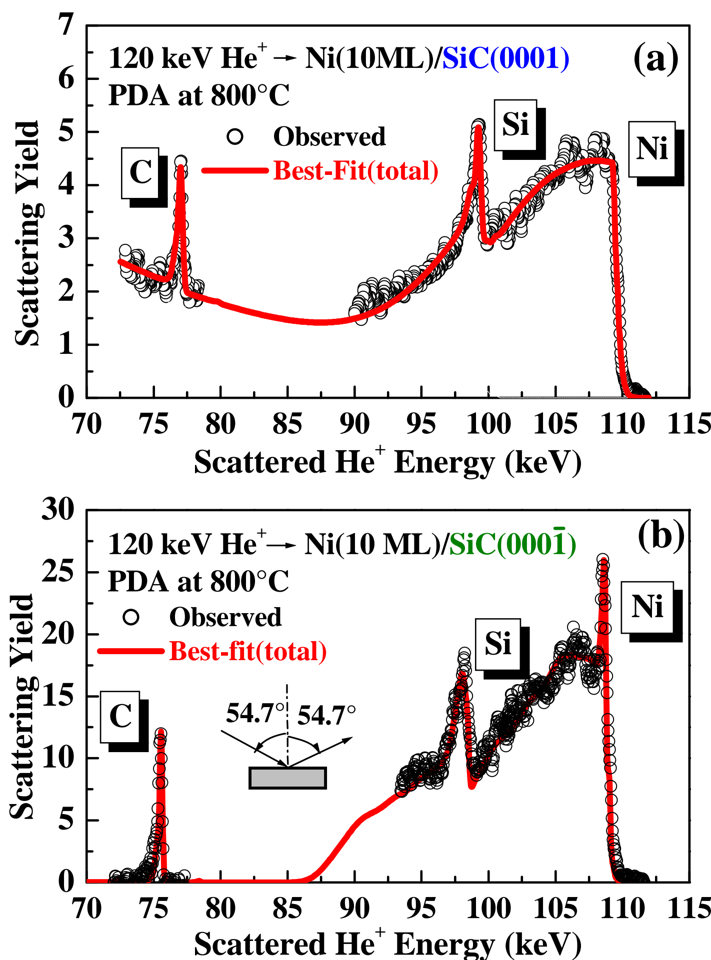

Fig. 3. MEIS spectra observed for (a) Ni(10 ML)/SiC(0001) and (b) Ni(10 ML)/ SiC($000\bar{1}$) annealed at 800°C for 2 min. Open circles and thick red-curves denote observed and best-fitted(total) spectra, respectively. Best-fit is obtained by assuming (a) islands occupancy of 37 % and islands consisting of $NiSi_2$(5×10^{15} atoms/cm^2) on top and NiSi with average thickness of 6.9×10^{16} atoms/cm^2 and standard deviation of 30 % and (b) islands occupancy of 35 % and islands consisting of Ni(0.3×10^{15} atoms/cm^2) on top and NiSi with average thickness of 6.4×10^{16} atoms/cm^2 and standard deviation of 25 %.

and (b) indicate magnified MEIS spectra from C atoms on the Si- and C-terminated substrates, respectively. Assumption of double-layer grapthite (DG) gives the best-fit to the observed C spectrum from the Si-terminated substrate, while the observed C spectrum from C-terminated substrate is reproduced assuming single-layer graphite (SG). The present MEIS analysis shows that Si atoms of ~10 (Si-C or C-Si) bilayers reacted with the deposited Ni atoms to grow NiSi islands and the residual C atoms formed DG on the Si-face and SG on the C-face. The areal density of graphene (3.82×10^{15} atoms/cm^2) is about triple that of SiC(0001) and thus ~4 ML of C for SiC(0001) and ~7 ML of C for SiC($000\bar{1}$) were lost, which were probably diffused into the bulk SiC lattices.

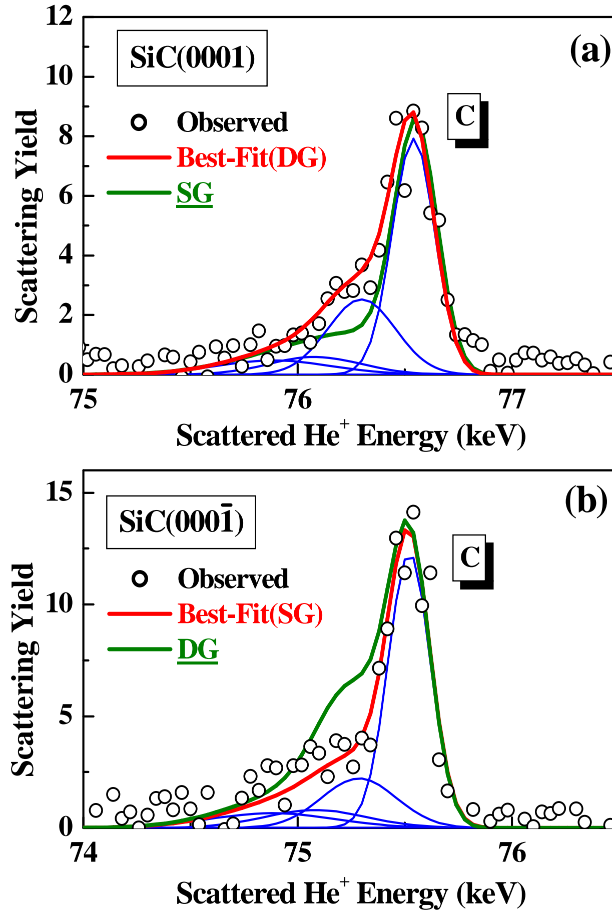

Fig. 4. Magnified MEIS spectra from C for (a) SiC(0001) and (b) SiC$(000\bar{1})$ substrates. Thick red-curves are the best-fit spectra assuming (a) double-layer of graphite (DG) for Si-face and (b) single-layer of graphite (SG) for C-face. Thin blue-curves originate from underlying SiC substrates. Thick green-curves are obtained assuming SG for Si-face and DG for C-face.

Growth of graphite layers was also revealed by C 1s core level spectra, as shown in Fig. 5. It is interesting that the E_B value of C 1s from SG/SiC($000\bar{1}$) is higher by 0.5 eV than that of DG/SiC(0001). Such a higher E_B value for SG than DG by 0.5 eV coincides with those observed

for the SG and DG grown on TaC(111)[11] and on Ni(111)[12] (see Table 1). This suggests that an electronic charge transfer occurs efficiently at the SG/support interfaces but not at DG/supports. Here, we set the E_B value of C 1s of SiC at 283.0 eV. From the C 1s intensity ratio of SiC/Graphite, it is possible to estimate roughly the thickness of the graphite using the escape depths for photoelectrons (~100 eV) in graphite and SiC. Using the escape depths predicted by Tanuma et al.[27,28], the thickness of the graphite on SiC(0001) and SiC($000\bar{1}$) were derived to be ~2.2 and ~1.6 ML, respectively. Because of the ambiguity of escape depths, the graphite thickness determined by MEIS is more reliable.

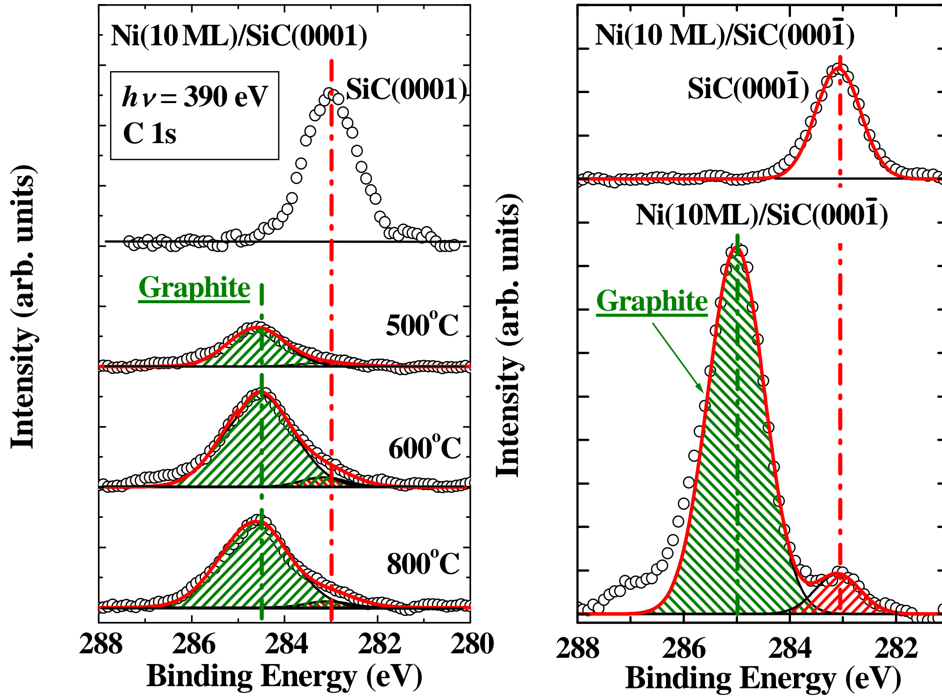

Fig. 5. C 1s core level spectra observed at photon energy of 390 eV under normal emission condition. Open circles and red-curves denote observed spectra and best-fitted total spectra, respectively for Si-face (left) and for C-face (right). Green and red straight lines indicate binding energy of C 1s from graphite and from bulk SiC, respectively.

We measured ultraviolet photoelectron spectra (UPS) at a photon energy of 40 eV for the ordered graphite layers and determined dispersion of the π band by varying the detection angle for emitted photoelectrons. The UPS spectra observed for the DG/SiC(0001) and SG/SiC($000\bar{1}$) at the $[1\bar{1}00]$ and $[11\bar{2}0]$ azimuth are shown in Fig. 6, as a function of detection angle. The dispersion curves along the $\bar{\Gamma}-\bar{M}$ and $\bar{\Gamma}-\bar{K}$ are obtained from the UPS spectra (Fig. 6) and shown in Fig. 7. The open and full triangles correspond to the DG/SiC(0001) and SG/SiC($000\bar{1}$), respectively. According to theoretical predictions for three-dimensional graphite, the π band ($2p_z$ basis orbitals) is

split into two branches originating from the overlap between $2p_z$ orbitals of neighboring layers[29,30]. However, the bonding between the graphite layers is too weak and thus a broad dispersion curve is usually observed. The present results are compared with those observed for SG/TaC(111) and DG/TaC(111)[11] and with theoretical dispersion curves based on the modified first principles Korringa-Kohn-Rostocker approach[29]. The dispersion curve for the DG/SiC(0001) coincides with the DG/TaC(111)[11] and with the lower branch given by the first principles calculations[29]. On the other hand, that for the SG/SiC($000\bar{1}$) takes significantly higher E_B values than those for the DG/SiC(0001) about 1 eV around the $\bar{\Gamma}$ point and lies more than 1 eV above the curve observed for the SG/TaC(111). The present result that the dispersion curve for SG on SiC is below that for DG/SiC is consistent with the fact that the π-band dispersion for SG/TaC(111) is below that for DG/TaC(111) (see Table 1).

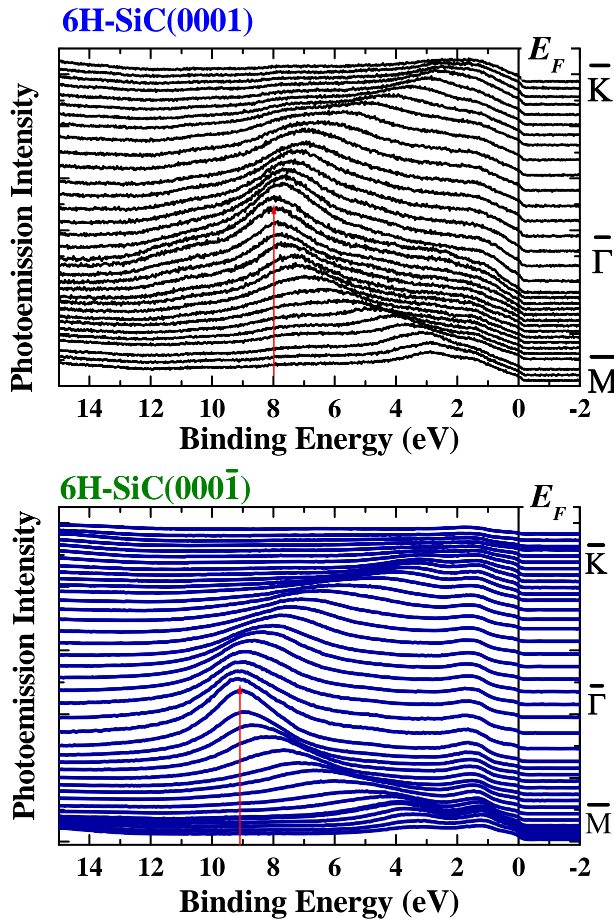

Fig. 6. Valence band spectra observed at photon energy of 40 eV for DG on Si-face (upper) and SG on C-face (bottom) varying emission angle from 0 to 35° with respect to surface normal.

Recently, Emtsev et al.[14] observed valence band and C 1s core level spectra for ultra-thin graphite layers grown on SiC(0001) and SiC($000\bar{1}$) substrates by annealing at 1150 - 1400°C in

UHV and concluded that the $6\sqrt{3}\times 6\sqrt{3}$ reconstruction(a precursor phase of graphitization) whose C atoms are bonded to the underlying Si atoms still remains at the interface during subsequent growth of graphite layers on SiC(0001), while the interaction between graphene and the SiC($000\bar{1}$) substrate is weak. This is in contradiction to the present results. Indeed, we observed the RHEED patterns from SiC(0001)-1×1 and graphite with double domains (graphite-[$1\bar{1}00$]//SiC-[$11\bar{2}0$]: dominant) but not from the $6\sqrt{3}\times 6\sqrt{3}$ structure. In the present case, Ni(10 ML)/SiC(0001) was annealed in UHV for 2 min at 800°C, which is much lower than the temperature (above 1150°C) for growth of the $6\sqrt{3}\times 6\sqrt{3}$ reconstruction and the silicidation reactions allow for growth of graphene at much lower temperatures and thus the interface structure is probably different from that of direct heating only at high temperatures. The graphenes obtained here probably consist of small double-domains compared with those formed by direct heating only[31]. Aside from the above inconsistency for graphene/SiC(0001), the π-band dispersion observed here for SG/SiC($000\bar{1}$) is consistent with that reported by Emtsev et al.[14].

Table 1. Observed C 1s binding energy (E_B), E_B at Γ point and work functions.

	C 1s E_B (eV)	E_B at Γ (eV)	Work Function (eV)
DG/SiC(0001)	284.5	8.2	4.25 (4.33 [16])
SG/SiC($000\bar{1}$)	285	9.2	5.15 (5.33 [16])
SG/Ni(111) [12]	285	10.3	3.9
SG/TaC(111) [11]	285	10.0	3.7
DG/TaC(111) [11]	284.5	8.5	4.2
Bulk graphite	284.5[11] (Present)	8.0[32]	4.6[11], 4.4[33] 4.2(Present)
$6\sqrt{3}\times 6\sqrt{3}$ SG/SiC(0001) SG/SiC($000\bar{1}$) [14]	284.75, 285.55 284.6 284.6	~12 ~8.5 ~9	

It was pointed out that the electronic states of monolayer-graphene is modified pronouncedly by hybridization of the π orbitals with the *d* orbitals of substrates such as TaC(111)[11] and Ni(111)[12]. Indeed, as presented before the electronic states of the SG on SiC($000\bar{1}$) as well as on TaC(111)[11] and Ni(111)[12] are quite different from those of bulk graphite. Quite recently, Mattausch and Pankratov[16] calculated the interface electronic states of graphene on Si- and C-terminated 6H-SiC(0001) substrates assuming a $\sqrt{3}\times\sqrt{3}-R30^{\circ}$ surface unit cell of graphite. Note that the orientation of the dominant domains of the SG on SiC($000\bar{1}$) and DG on SiC(0001) coincides with that of the $\sqrt{3}\times\sqrt{3}-R30^{\circ}$ reconstruction. They predicted a metallic interface for graphene on the Si-face, whereas semiconducting or semimetallic interface for single or double graphene on the C-face, respectively. Note that if the $6\sqrt{3}\times 6\sqrt{3}$ structure exists on the SiC(0001), the interface

is semiconducting[14]. It was also demonstrated that the work functions of graphene on the C-face are much lager than those of graphene on the Si-face[16]. We measured secondary electrons spectra at 140 eV of photon incident on the DG/SiC(0001) and SG/SiC($000\bar{1}$) which were biased negatively (V). The secondary electron intensity rises steeply at $E_{kin}{}^{0}$, as shown in Fig. 8 (a). The work function (Φ) is deduced by the following relation,

$$\Phi = E_{kin}{}^{0} + \Phi_{SP} - |V|, \tag{1}$$

where Φ_{SP} is the work function of the spectrometer (3.80 eV). Note that the areal occupation ratio of the SG and DG graphene is ~65 % and the secondary electron intensity for HOPG is much larger than that for NiSi near the $E_{kin}{}^{0}$ value (see Fig. 8 (c)) and thus the observed spectra originate mainly from the graphene regions. The observed work functions for the DG/SiC(0001) and SG/SiC($000\bar{1}$) are 4.25±0.05 and 5.15±0.05 eV, respectively, which are in excellent agreement with the theoretical predictions (4.33 and 5.33 eV)[16]. Such characteristic electronic states of graphene dependent on its thickness and underlying substrates are crucial points in the prospect of graphene-based nanometer-scale electronic devices.

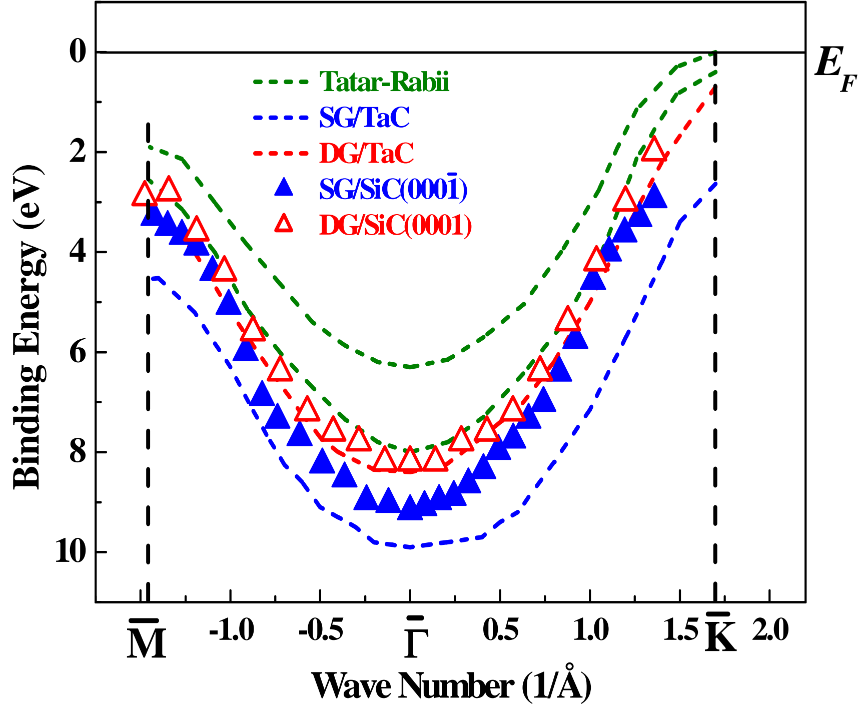

Fig. 7. π band dispersion observed for DG/SiC(0001) (open red-triangles) and SG/ SiC($000\bar{1}$) (full blue-triangles). Red and blue dashed-curves denote the dispersion curves observed for DG and SG on TaC(111), respectively[11]. Green dashed-curves are calculated ones by Tatar and Rabii[29].

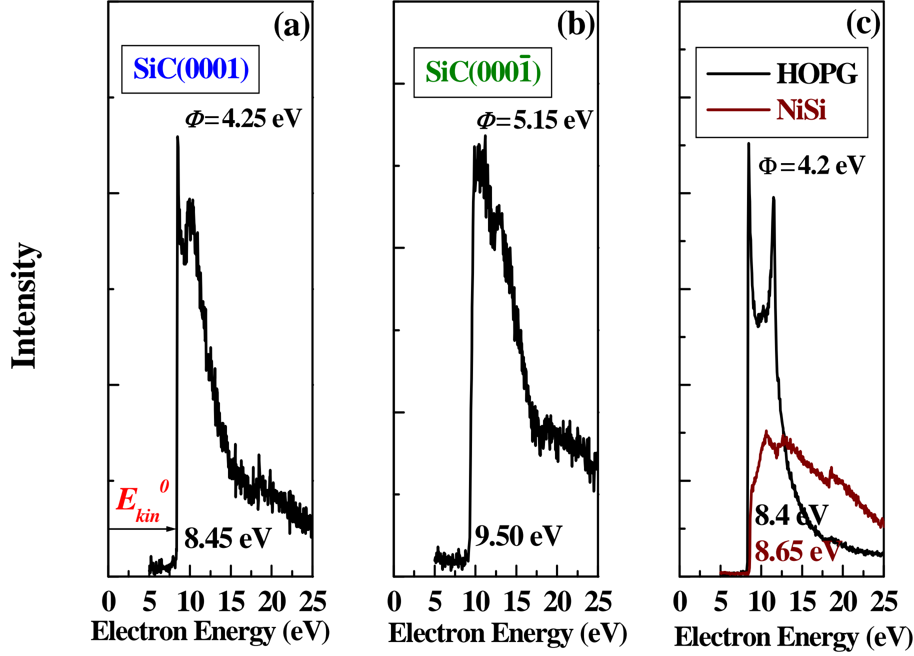

Fig. 8. Secondary electrons spectra observed at photon energy of 140 eV for (a) DG/SiC(0001), (b) SG/ SiC$(000\bar{1})$ and (c) HOPG (black curve) and NiSi/Si(111) (green curve). Negative bias of 8.0, 8.15 and 8.0 V were applied to (a), (b) and (c) samples, respectively.

4. Summary

The silicidation reactions taking place on Ni(10ML)/6H-SiC(0001)-$\sqrt{3}\times\sqrt{3}$ and Ni(10ML)/6H-SiC$(000\bar{1})$-2×2 substrates were studied *in situ* by RHEED, high-resolution MEIS and photoelectron spectroscopy using SR light. Epitaxial Ni layers grow at RT on both substrates in spite of a large lattice mismatch of 19 %. This is due to the diffusion of Si atoms into the Ni lattices, which are supplied from the reconstructed Si adlayers and adatoms for C-face and from the reconstructed Si adatoms and the first Si-C bilayer for Si- face. Ni-silicidation reactions occur at temperatures higher than 400°C and a single-phase θ-Ni_2Si(0001) layer grows epitaxially at 500°C on the C-face, while a mixed phase (Ni_2Si + NiSi + $NiSi_2$) layer is formed on the Si-face.

Annealing at 800°C for 2 min leads to formation of Ni-silicide islands (areal occupation ratio: ~35 %) with average composition ratio of Si/Ni = 1, which are surrounded by ordered graphite layers. High-resolution MEIS analysis revealed that DG grew on the Si-face and SG on the C-face. Such a significant difference in the growth modes of Ni-silicides and graphene is due to a faster reaction rate for Ni with Si-C bilayer than with C-Si bilayers. It is probably possible to control the thickness of the ordered graphite layers on the Si- and C-faces by choosing appropriately Ni thickness, annealing temperature and annealing time. The E_B value of C 1s for the SG/SiC$(000\bar{1})$ is larger by 0.5 eV than that for the DG/SiC(0001), coinciding with the E_B values of C 1s observed for SG and DG on

TaC(111). This suggests an electronic charge transfer taking place more efficiently between SG and SiC substrate than that between DG and SiC. The dispersion curve (π-band) for the DG/SiC(0001) is in good agreement with the DG/TaC(111) and with the lower branch given by the first principles calculations. The π-band for the SG/SiC($000\bar{1}$) lies about 1 eV above the curve for the DG/SiC(0001) around the $\bar{\Gamma}$ point. The π-band dispersion for the SG/SiC($000\bar{1}$) observed here is consistent with that reported by Emtsev et al.[14]. We also measured the work functions (Φ) of the DG/SiC(0001) and SG/SiC($000\bar{1}$) and found that the Φ value of 4.25±0.05 eV for the DG/SiC(0001) was considerably smaller than that of 5.15±0.05 eV for the SG/SiC($000\bar{1}$). The above Φ values agree quite well with the theoretical predictions based on the *ab initio* density functional calculations. The present results indicate that the electronic properties of graphene are significantly affected by the interaction with the substrate.

Acknowledgements

The authors would like to thank Dr. M. Takizawa for his support in the PES experiments. Special thanks are due to our colleagues, T. Nishimura, S. Matsumoto and Y. Matsubara for their kind assistance throughout our experiments. Useful comments of Dr. Y. Maeda on work functions is gratefully acknowledged. This work is partly supported by Ministry of Education, Culture, Sports, Science and Technology, MEXT, 2007-2011.

References

[1] K.S. Novoselov, A.K. Geim, S.V. Morozov, D. Jiang, Y. Zhang, S.V. Dubonos, I.V. Grigorieva and A.A. Firsov, Science **306** (2004) 666.
[2] Y. Zhang, J.P. Small, W.V. Pontius and P. Kim, Appl. Phys. Lett. **86** (2005) 073104.
[3] K.S. Novoselov, A.K. Geim, S.V. Morozov, D. Jiang, M.I. Katsnelson, I.V. Grigorieva, S.V. Dubonos and A.A. Firsov, Nature **438** (2005) 197.
[4] Y. Zhang, Z. Jiang, J.P. Small, M.S. Purewal, Y.-W. Tan, M. Fazlollahi, J.D. Chudow, J.A. Jaszczak, H.L. Stormer and P. Kim, Phys. Rev. Lett. **96** (2006) 136806.
[5] T. Ohta, A. Bostwick, T. Seyller, K. Horn and E. Rotenberg, Science **313** (2006) 951.
[6] J. Hass, R. Feng, T. Li, X. Li, Z. Zong, W.A. de Heer, P.N. First, E.H. Conrad, C.A. Jeffrey and C. Berger, Appl. Phys. Lett. **89** (2006) 143106.
[7] T. Ohta, A. Bostwick, J.L. McChesney, T. Seyller, K. Horn and E. Rotenberg, Phys. Rev. Lett. **98** (2007) 206802.
[8] K. Kobayashi, Phys. Rev. **B 48** (1993) 1757.

[9] K. Nakada and M. Fujita, Phys. Rev. **B 54** (1996) 17954.
[10] K. Sugawara, T. Sato, S. Souma, T. Takahashi and H. Suematsu, Phys. Rev. **B 73** (2006) 045124.
[11] A. Nagashima, H. Itoh, T. Ichinokawa and C. Oshima, Phys. Rev. **B 50** (1994) 4756.
[12] A. Nagashima, N. Tejima and C. Oshima, Phys. Rev. **B 50** (1994) 17487.
[13] I. Forbeaux, J.-M. Themlin and J.-M. Debever, Phys. Rev. **B 58** (1998) 16396.
[14] K. Emtsev, F. Speck, Th. Seyller, L. Ley and J.D. Riley, Phys. Rev. **B 77** (2008) 155303.
[15] Y. Hoshino, S. Matsumoto, T. Nakada and Y. Kido, Surf. Sci. **556** (2004) 78.
[16] A. Mattausch and O. Pankratov, Phys. Rev. Lett. **99** (2007) 076802.
[17] A. Grüneis, C. Attaccalite, L. Wirtz, H. Shiozawa, R. Saito, T. Pichler and A. Rubio, Phys. Rev. **B 78** (2008) 205425.
[18] W. Kern and D.A. Puotinen, RCA Rev. **31** (1970) 187.
[19] Y. Hoshino, S. Matsumoto and Y. Kido, Phys. Rev. **B 69** (2004) 155303.
[20] J.F. Ziegler, J.P. Biersack and W. Littmark, *The Stopping and Range of Ions in Matter* (Pergamon, New York, 1985).
[21] J. Lindhard and M. Scharff, Kgl. Danske. Vidensk. Selsk. Mat. –Fys. Medd. **27** (15)(1953) 1.
[22] M. Hazama, Y. Kitsudo, T. Nishimura, Y. Hoshino, P.L. Grande, G. Schiwietz and Y. Kido, Phys. Rev. **B 78** (2008) 193402.
[23] Y. Hoshino, Y. Matsubara, T. Nishimura and Y. Kido, Phys. Rev. **B 72** (2005) 235416.
[24] K. Maex and M. Van Rossum, *Properties of Metal Silicides* (Short Run Press Ltd., Exter, 1995).
[25] P.J. Grunthaner, E.J. Grunthaner, J.W. Mayer, J. Vac. Sci. Technol. **17** (1980) 924.
[26] L. Gregoratti, S. Günther, J. Kovac, M. Marsi and M. Kishinova, Surf. Sci. **439** (1999) 120.
[27] S. Tanuma, C.J. Powell and D.R. Penn, Surf. Int. Anal. **20** (1993) 77.
[28] S. Tanuma, T. Shiratori, T. Kimura, K. Goto, S. Ichimiya and C.J. Powell, Surf. Int. Anal. **37** (2005) 833.
[29] R.C. Tatar and S. Rabii, Phys. Rev. **B 25** (1982) 4126.
[30] A. Grüneis, C. Attaccalite, L. Wirtz, H. Shiozawa, R. Saito, T. Pichler and A. Rubio, Phys. Rev. **B 78** (2008) 205425.
[31] C. Reidl, U. Starke, J. Bernhardt, M. Franke and K. Heinz, Phys. Rev. **B 76** (2007) 245406.
[32] T. Takahashi, H. Tokailin and T. Sagawa, Phys. Rev. **B 32** (1985) 8317.
[33] H. Ago, T. Kugler, F. Cacialli, W.R. Salaneck, M.S. Shafer, A.H. Windle and R.H. Friend, J. Phys. Chem. **103** (1999) 8116.